

Genesis and trends in marine heatwaves over the tropical Indian Ocean and their interaction with the Indian summer monsoon

J. S. Saranya^{1,2}, M K Roxy^{1*}, Panini Dasgupta^{1,3} and Ajay Anand^{1,4}

¹*Centre for Climate Change Research, Indian Institute of Tropical Meteorology, Pune 411008, India*

²*College of Climate Change and Environmental Sciences, Kerala Agricultural University, Kerala, 680656, India*

³*Department of Meteorology and Oceanography, College of Science and Technology, Andhra University, Visakhapatnam, Andhra Pradesh 530003, India*

⁴*Department of Atmospheric Sciences, Cochin University of Science and Technology, Kerala, 682022, India*

Key points:

- An increasing trend in marine heatwaves is observed over the western Indian Ocean and the Bay of Bengal.
- Ocean warming and El Niño events drives the genesis and trends of marine heatwaves in the Indian Ocean.
- Marine heatwaves are reducing the monsoon rainfall over the central Indian subcontinent while enhancing it over the southern peninsula.

JGR Oceans, submitted on 31 March 2021

*Corresponding author address: Roxy Mathew Koll, Indian Institute of Tropical Meteorology, Pune 411008, India. E-mail: roxy@tropmet.res.in

1 **Abstract**

2 Marine heatwaves (MHWs) are extreme oceanic warm water events (above 90th percentile threshold)
3 that significantly impact the marine environment. Several studies have recently explored the genesis
4 and impacts of MHWs though they are least understood in the tropical Indian Ocean. Here we
5 investigate the genesis and trend of MHWs in the Indian Ocean during 1982–2018 and their role in
6 modulating the Indian monsoon. We find that the rapid warming in the Indian Ocean plays a critical
7 role in increasing the number of MHWs. Meanwhile, the El Niño has a prominent influence on the
8 occurrence of MHWs during the summer monsoon. The Indian Ocean warming and the El Niño
9 variability have synergistically resulted in some of the strongest and long-lasting MHWs in the Indian
10 Ocean.

11 The western Indian Ocean (WIO) region experienced the largest increase in MHWs at a rate of
12 1.2–1.5 events per decade, followed by the north Bay of Bengal at a rate of 0.4–0.5 events per decade.
13 Locally, the MHWs are induced by increased solar radiation, relaxation of winds, and reduced
14 evaporative cooling. In the western Indian Ocean, the decreased winds further restrict the heat transport
15 by ocean currents from the near-equatorial regions towards the north. Our analysis indicates that the
16 MHWs in the western Indian Ocean and the north Bay of Bengal lead to a reduction in monsoon rainfall
17 over the central Indian subcontinent. On the other hand, there is an enhancement of monsoon rainfall
18 over southwest India due to the MHWs in the Bay of Bengal.

19

20 **Plain Language Summary**

21 Marine heatwaves are periods of extremely high temperatures in the ocean. Though several studies
22 have reported their occurrence and impacts in the global oceans, they are least understood in the
23 tropical Indian Ocean. In the current study, we find that marine heatwaves are increasing in the Indian
24 Ocean, with the largest increase observed over the western Indian Ocean, followed by the north Bay
25 of Bengal. These marine heatwaves occur as a result of background ocean warming in the Indian Ocean

and also in response to El Niño events in the Pacific Ocean. Locally, a peak in solar radiation and a dip in evaporative cooling due to weak winds lead to the formation of these marine heatwaves. In the western Indian Ocean, the weak winds also reduce the heat transported by ocean currents from the near-equatorial regions towards the north, intensifying the marine heatwave. In turn, these marine heatwaves impact the monsoon by reducing the rainfall over the central Indian subcontinent while enhancing it over the southern peninsula.

1. Introduction

According to the Special Report on the Ocean and Cryosphere (SROCC) of the Intergovernmental Panel on Climate Change (IPCC), the global ocean will continue to warm during the 21st century (IPCC, 2019). By 2100, the ocean warming in the top 2000 m is estimated to be 5–7 times higher under the business-as-usual scenario and 2–4 times higher under the low emission scenario, relative to the temperature reported since 1970 (*very likely*). Under this warming scenario, a rise in extreme temperature events in the ocean is also projected. Marine heatwaves (MHWs) are anomalous warm water events a response to the warming ocean—defined when the daily sea surface temperature (SST) exceeds the 90th percentile for five or more days (percentile threshold may vary and can be as high as the 99th percentile) (Hobday et al., 2016, Schaeffer et al., 2017, Collins et al., 2019). MHWs are reported all over the world—the 2003 Mediterranean Sea MHW, 2011 West Australian MHW, 2015/16 Tasman Sea MHW are some of them. Numerous studies indicate that these anomalous temperature events can cause habitat destruction due to coral bleaching, seagrass destruction, and loss of kelp forests, affecting the fisheries sector adversely (Mills et al., 2013, Collins et al., 2019).

Numerous studies have focused on the mechanisms leading to the genesis of MHWs. Most of the MHWs in Indo-Pacific regions are associated with climate modes like the El Niño, the Indian Ocean Dipole (IOD), and the Pacific Decadal Oscillation (PDO). The 2014–2015 MHW in the Northeast Pacific was associated with the PDO and the North Pacific Gyre Oscillation (NPGO). These

51 modes enhanced the conditions that led to an increase in SST in the Northeast Pacific (Joh and Lorenzo,
52 2017). Holbrook et al. (2019) had suggested that the SST variability in the tropical Indian and Pacific
53 oceans is related to the El Niño, IOD, and Indian Ocean warming.

54 Although several studies have explored the extreme temperature events in the Pacific and
55 Atlantic oceans, there is hardly any in-depth research on MHWs in the Indian Ocean. In the southeast
56 Indian Ocean, coral bleaching due to the MHWs was reported, mostly associated with the El Niño and
57 Madden-Julian Oscillations (MJO), riding over a global warming signal (Zhang et al., 2017). Studies
58 have reported high SST conditions in the western Indian Ocean (Seychelles region), Arabian Sea, and
59 the Bay of Bengal region (Andaman Sea) and also point out the coral bleaching due to intense warming
60 in these regions (Saji et al., 1999; Edward et al., 2018; Raj et al., 2018; Krishnan et al., 2011).

61 The north Indian Ocean is a critical region because it supports large marine primary
62 productivity, particularly during the South Asian summer monsoon (Roxy et al., 2016), and because
63 of its role in modulating the intraseasonal and interannual variability of the monsoon (Roxy et al.,
64 2007, 2012; Singh and Dasgupta 2017). Understanding the genesis and evolution of MHWs during the
65 summer monsoon season and their changes due to ocean warming is hence crucial. In this study, for
66 the first time, we explore the genesis and trend of MHWs in the Indian Ocean during the summer
67 monsoon season (June–September). While many studies have addressed the impacts of MHWs on the
68 marine ecosystem, there are hardly any studies investigating the impacts of MHWs on atmospheric
69 circulation and rainfall. Hence, we investigate the interaction between MHWs and Indian summer
70 monsoon circulation and rainfall.

71

72 **2. Data and methods**

73 **2.1 Data**

74 To identify the MHWs, we used the Optimum Interpolated Sea Surface Temperature (OISST) dataset
75 at a resolution of $0.25^\circ \times 0.25^\circ$ (Reynolds et al., 2007). In order to study the impact of MHWs on

76 atmospheric conditions, we used the NOAA Interpolated Outgoing Longwave Radiation (OLR)
77 measured from Advanced Very High-Resolution Radiometer (AVHRR) onboard NOAA polar-
78 orbiting spacecraft (Liebmann and Smith, 1996), at a $2.5^\circ \times 2.5^\circ$ resolution. The daily wind, latent heat
79 flux, sensible heat flux, upward longwave radiation, downward solar radiation, surface net longwave
80 radiation, and surface net solar radiation are obtained from the National Center for Environmental
81 Prediction/National Centers for Atmospheric Research (NCEP/NCAR) reanalysis data at a resolution
82 of $2.5^\circ \times 2.5^\circ$ (Kalnay et al., 1996). For the analysis of the rainfall variability over the India, we used
83 IMD daily rainfall at a resolution of $0.25^\circ \times 0.25^\circ$ (Pai et al., 2014). All the analyses are compared
84 with European Centre for Medium-Range Weather Forecasts (ECMWF) ERA5 reanalysis product
85 (Hersbach and Dee, 2016). In the main text, we use NCEP/NCAR products, and in the supplementary
86 information, we compare our results with ERA5 reanalysis products.

87 To investigate the ocean conditions during the MHWs, we obtained the ocean current data at
88 $1/3^\circ$ grid with a five-day temporal resolution from the Ocean Surface Current Analysis Real-time
89 (OSCAR) (Dohan and Maximenko, 2010). The monthly potential temperature and salinity are obtained
90 from ORAS4 at a horizontal resolution of $1^\circ \times 1^\circ$ (Balmaseda et al., 2013). Apart from this, daily water
91 temperature and salinity are obtained from the Hybrid Coordinate Ocean Model (HYCOM) reanalysis.
92 We supplemented the heat budget analysis using the HYCOM reanalysis (Metzger et al., 2014) at a
93 resolution of $1/12^\circ$ for 1994–2015.

94

95 **2.2 Methods**

96 **2.2.1 Detection of marine heatwaves**

97 In this study, we identify MHWs from the OISST daily datasets, where the SST is above the 90th
98 percentile (threshold) and persist for at least five days. The threshold and climatology are seasonally
99 varying and calculated using daily temperature data, setting a day-centered 11-day window and a 31-
100 day moving window for smoothing. We also utilize specific matrices to study and analyze the MHWs,

such as the maximum intensity (maximum temperature anomaly during a particular event), mean intensity (mean temperature anomaly during a specific event), cumulative intensity (sum of temperature anomaly during a particular event), duration (number of days between the starting and ending dates), and spatial extent (area covered by MHW event) (Hobday et al., 2016). To study the spatial extent of the MHWs, we counted the grids where the MHW events occurred and multiplied them by the grid area. To estimate the trend in MHWs, we used the OISST data from 1982–2018 and calculated MHW at each grid, and then fit a linear trend model. Along with the annual values, we also prepare the MHW metrics for June to September.

Further, we did a composite analysis of wind, SST, latent heat flux, sensible heat flux, upward longwave radiation, and downward solar radiation during one week before and after the starting date of MHW events. This provides us with a comprehensive picture of the genesis of MHWs and describes the physical and dynamical processes involved with the MHW genesis over the particular regions. To study the interaction between the MHWs and summer monsoon circulation and rainfall, we have included a composite analysis of wind at 850 hPa, OLR, omega at 500 hPa, vertically integrated moisture flux, and rainfall over India during the MHWs.

2.2.2 Mixed layer heat budget

To study the local factors influencing the genesis of MHWs, we estimated the mixed layer heat budget using the temperature tendency equation. The temperature tendency equation gives us a comprehensive picture of factors that lead to the change in the ocean surface temperature (Rodrigues et al., 2019). The temperature tendency equation is given by

$$\partial T_m / \partial t = -v \cdot \nabla T + Q_0 / \rho C_p H_m + Res \quad (1)$$

where ρ is the density of seawater ($1,026 \text{ kg m}^{-3}$), and C_p is the specific heat of seawater ($3902 \text{ J kg}^{-1} \text{ K}^{-1}$), and T_m is the mixed layer temperature. Here we have used the SST as a mixed layer temperature because the vertically averaged mixed layer temperature is close to the SST values (Foltz et al., 2003).

126 $\partial T_m / \partial t$ represents the rate of change of mixed layer temperature. The term $-v \cdot \nabla T$ indicates the advection
 127 and v indicate the horizontal velocity vector (v at 15m depth from OSCAR Ocean currents, vertically
 128 averaged over the mixed layer). H_m means the mixed layer depth (MLD) in meters. Using the monthly
 129 potential temperature and salinity data of ORAS4, we calculated the monthly MLD as the depth at
 130 which the density changes by a threshold of 0.05 kg m^{-3} for depth of 5 m. The monthly MLD is
 131 interpolated in to daily to estimate the heat flux terms (Rodrigues et al., 2019).

$$132 \quad Q_0 = Q_s + Q_b + Q_e + Q_h \quad (2)$$

133 Q_0 is the net surface heat flux (W m^{-2}), which includes the latent heat flux Q_e , and the sensible heat
 134 flux Q_h released from the ocean mixed layer, the net solar radiation received Q_s , and the net longwave
 135 radiation released Q_b . Finally, the *Res* include the remaining unresolved process, such as vertical
 136 diffusion, and entrainment. The heat budget analysis is also verified with HYCOM ocean current
 137 datasets. All the heat budget terms are calculated from 1994–2015 for the two study regions and
 138 averaged over that region. Anomalies are derived from the 1994–2015 daily climatology. Then we
 139 estimate the heat budget terms for the five days before the start date of MHWs in the selected regions.

140

141 **3. Results**

142 To investigate the changes in MHWs in the Indian Ocean, we first select those regions in the tropical
 143 Indian Ocean that experienced an increasing trend in MHWs during 1982–2018. The result section is
 144 organized into five sections. Section 3.1 describes the MHWs in the Indian Ocean and their trend. In
 145 section 3.2, we describe the seasonal climatology of MHWs for the regions where the trends are the
 146 largest. Section 3.3 addresses the role of dominant modes of climate variability on the MHWs in the
 147 tropical Indian Ocean. In section 3.4, we focus on the genesis and evolution of MHWs during the
 148 southwest monsoon season (June–September) and then describes the interaction between MHWs and
 149 the monsoon rainfall in section 3.5.

150

3.1 Observed trends in marine heat waves in the Indian Ocean

The trend in the annual MHW frequency from 1982–2018 over the Indian Ocean is shown in Figure 1a. The western Indian Ocean region (41°E–56°E, 8°S–8°N) shows the most prominent trend in MHWs, annually. The western Indian Ocean region has an increasing trend of 1.2–1.5 MHW events per decade ($p < 0.01$) at each grid point. The northern Arabian Sea also shows a similar increasing trend. Meanwhile, in the eastern Indian Ocean and central equatorial Indian Ocean (80°E–110°E, 0°–20°S), the trend is about 0.4 MHW events per decade.

The boreal summer monsoon months (June–September) are immensely crucial for the Indian Ocean rim countries because the rainfall during this season supports the food, water, and energy security of this region (Beal et al., 2020; Wang et al., 2020). SST variability in the tropical Indian Ocean regulates the monsoon circulation and rainfall. Recognizing the importance of the SSTs during the northern summer monsoon months, we investigate the changes in MHWs during this season (June–September), for 1982–2018 (Figure 1b). During June–September, there are two regions where MHWs activities are rapidly increasing. One is in the western Indian Ocean region, where the annual trend in MHWs frequency is also maximum. The second one is in the northern Bay of Bengal (85°E–93°E, 15°N–23°N) region. These two regions are experiencing an increasing trend of 0.5 events per decade during June–September. Apart from these two locations, the northeastern Arabian Sea also shows a similar increasing trend.

We further examined the month-wise trend of the frequency of MHWs over western Indian Ocean and northern Bay of Bengal region. For the western Indian Ocean region (in Figure 1c), we find that the increasing trend of MHW frequency is present in all months. The trend is most considerable in July to December, with the maximum in November. For the north Bay of Bengal region, the MHWs frequency trends are small in January to April and large in May to August, and moderate in September to December (Figure 1d). Hence, the western Indian Ocean region is crucial in the tropical Indian

175 Ocean, experiencing a significant increasing trend in the frequency of MHWs year-round, while the
176 north Bay of Bengal region is experiencing a significant trend during summer monsoon months.

177 Henceforth, we focus our analysis on the western Indian Ocean (41°E–56°E, 8°S–8°N) and
178 north Bay of Bengal (85°E–93°E, 15°N–23°N) regions, where the MHW trends are the largest. We
179 identified individual MHW events based on the spatial mean SST time series over western Indian
180 Ocean and north Bay of Bengal boxes in Figure 1b. There are 66 MHW events that occurred in the
181 western Indian Ocean region during the 1982–2018 period, in which 21 events occurred during June–
182 September. The north Bay of Bengal region witnessed 94 MHW events, and 34 out of these occurred
183 during June–September. The time series of the annual and monsoon MHW frequency for western
184 Indian Ocean and north Bay of Bengal are shown in Figure 1e, f. Every year, the MHWs numbers are
185 increasing significantly at a rate of 0.14 annual events per year for western Indian Ocean and 0.09
186 annual events per year for the north Bay of Bengal over the 1982–2018 period. On the other hand, the
187 MHW frequency during the monsoon season is increasing at a rate of 0.04 events per year in the
188 western Indian Ocean region and 0.05 events per year in the north Bay of Bengal (Figure 1 e, f). It is
189 evident from the time series that the trend of MHW frequency in the north Bay of Bengal during June–
190 September shows higher values compared to the western Indian Ocean region during the same period.

191

192 **3.2 Seasonal climatology of marine heatwaves in the tropical Indian Ocean**

193 For the western Indian Ocean region, all the MHW metrics (Figure 2) show a double peak in the
194 seasonal climatology signal during March and September months. During these two months, the
195 duration of MHWs may reach 40 and 60 days, respectively. The mean intensity shows high seasonal
196 variability. The mean intensity during March and September is highest with a mean value of 1.1°C. In
197 the case of maximum intensity, it is 1.4°C during the peak months. In the case of area covered by the
198 MHW events, it is 2 million km² during the peak months of March and September.

199 For the north Bay of Bengal, the cumulative intensity and duration exhibit a peak during
200 February, while the peak in the area, mean intensity, and maximum intensity is in May. Further, the
201 number of events is maximum during May and October months (12 and 14 events respectively). The
202 seasonal signal of MHW metrics in the north Bay of Bengal shows peak values either in February or
203 May. The cumulative intensity and duration in the peak month of February are 16°C days and 18°C
204 days, respectively. The mean intensity during the May month is 1.1°C, while the maximum intensity
205 is 1.3°C. During the peak month, the area is 0.45 million km².

206

207 **3.3 Role of Indian Ocean warming and dominant modes of climate variability on marine** 208 **heatwaves**

209 Recent research on MHWs (Laufkötter, et al., 2020, Holbrook et al., 2019, Frölicher et al., 2018) and
210 the IPCC Special Report on Oceans and Cryosphere in a Changing Climate (SROCC) point out that
211 MHW events are a manifestation of the global warming trend (Collins et al., 2019). A pattern
212 correlation between the tropical SST trends and tropical MHW trends shows a significantly high
213 correlation ($r=0.8$ for annual values and $r=0.6$ for boreal summer season) supporting this argument.
214 Besides the global SST rise, various modes of climate variability favor MHW events by generating the
215 necessary background conditions.

216 This section investigates the role of different climate modes on the occurrences of MHW
217 events, particularly the association with El Niño, Indian Ocean basin-wide warming mode (IOB, Indo-
218 Pacific warming generally occurring during the post- El Niño periods), Indian Ocean Dipole (IOD),
219 and the North Atlantic Oscillation (NAO). Figure 3 shows the number of MHW days coincident with
220 these climate modes or overlapping modes. The absence of any climate modes during the MHW is
221 indicated as “Nil”.

222 Correlation and composite analysis of the yearly count of MHW days in the western Indian
223 Ocean region with the annual mean SSTs show that these events are associated with the El Niño, IOB

224 (Indian Ocean warming), and negative North Atlantic Oscillation (NAO) (Figure 3a, b). Out of all the
225 western Indian Ocean MHW days, the most significant number of MHW days occur under the Indian
226 Ocean warming condition (Figure 3a, b). There are a significant number of MHW days when no
227 climate modes are present. Regardless, there are a large number of MHW days under the positive IOD
228 and negative NAO conditions. The spatial correlation between the MHW days in the western Indian
229 Ocean region and mean SSTs for June–September shows significant associations with warm SSTs in
230 the western Indian Ocean and El Niño and IOD. Most of the MHW days in June–September occur
231 without any influence of climate modes (Figure 3d).

232 Similar to the western Indian Ocean region, correlation and composite analysis of the yearly
233 count of MHWs days in the north Bay of Bengal with the annual mean SST shows an association with
234 the Indian Ocean warming, El Niño, and negative NAO (Figure 3e, f). Out of all the north Bay of
235 Bengal MHW days, significant MHW days occur under the Indian Ocean warming condition. There
236 are several MHW days associated with the negative NAO conditions following the IOB condition.
237 Meanwhile, for June to September, the MHW days in the north Bay of Bengal appear to occur with
238 warming in the north Indian Ocean (Figure 3g) and negative NAO pattern (Figure 3h).

239 In summary, occurrences of western Indian Ocean and north Bay of Bengal MHWs are more
240 frequent while Indian Ocean warming is prominent basin wide (IOB) or when the western (for western
241 Indian Ocean MHWs in summer) or northern (for Bay of Bengal MHWs in summer) exhibits warming.
242 The western Indian Ocean SSTs also respond to the El Niño due to the subsidence of Walker circulation
243 over these regions (Roxy et al. 2014, Xie et al., 2016). This subsidence inhibits deep convection and
244 thereby suppresses the release of heat from the ocean to the atmosphere. Thus, the Indian Ocean attains
245 its maximum temperatures under the IOB mode. That is, the background warming in the Indian Ocean
246 has a strong influence on the MHWs in the Indian Ocean basin on an annual timescale. During a
247 positive IOD event, the western Indian Ocean becomes warmer than its climatology. June–September
248 MHWs in the western Indian Ocean region is often associated with these positive IODs. The negative

NAO phases are also associated with MHWs over the north Bay of Bengal region. However, the mechanism between the negative NAO and north Indian Ocean SST needed to be explored in detail.

251

3.4 Local ocean-atmospheric interaction leading to the genesis and evolution of MHW events

In this section we explore the role of local ocean-atmospheric conditions leading to the initiation and the persistence of MHWs in the Indian Ocean. It is observed that for the western Indian Ocean MHWs, the downward solar radiation leads the SST peak by ~10 days. However, this lead-lag relation is weak ($r=0.13$). The increased downward solar radiation due to clear sky conditions may increase SST in the western Indian Ocean region but is not the primary reason for MHW genesis. Meanwhile, the reduced wind speed and evaporation (denoted by the negative wind anomaly and reduced upward latent heat flux anomaly in Figure 4a) leads the SST anomalies by ~3 days ($r=-0.24$, $p<0.05$), assisting the MHW formation. Besides the air-sea fluxes, reduced wind speed also impacts the ocean current over the western Indian Ocean Region. The ocean currents in the western Indian Ocean region (driven by strong cross-equatorial monsoon winds) are usually strong and transport heat away from the equator. Hence, a weakening of the cross-equatorial winds can potentially reduce ocean heat transport by accumulating the heat in this region, enhancing the MHWs.

To comprehend the spatial distribution of the lead-lag relationship, composites of different variables from a week before and after the MHW genesis date are presented in Figure 4b. The SST anomalies show a dipole pattern with cold anomalies at 15°N and warm anomalies at the equator prior to the genesis of western Indian Ocean MHWs. In Figure 4a, the region of cold SST anomalies can be observed north of the western Indian Ocean region a week prior to the MHWs initiation. The warm SST anomalies near the equator gradually become prominent as the MHW initiates. Interestingly, the cold SST anomalies at the north of the western Indian Ocean region peaks 35~40 days prior to the MHWs genesis. The meridional SST difference between the north (15°N) and western Indian Ocean region also peaks 30 days earlier to the genesis of MHWs (supplementary information Figure S3).

274 These cold SST anomalies at 15°N and the meridional SST difference may have a significant role in
275 reducing the strength of cross-equatorial wind flow (Figure 4b). The reduced wind speed not only
276 reduces the air-sea fluxes (reduce evaporation) (Figure 4b) but also affects the strength of ocean
277 currents, leading to decreased heat transport from the equator towards the north. These factors
278 contribute to the MHW formation in the particular region. One week prior to the MHWs genesis, the
279 clear sky condition over the western Indian Ocean region due to the weak cross-equatorial flow and
280 less evaporation increases downward solar radiation. The increase in downward solar radiation further
281 increases the SST. Therefore, from the lead-lag time series and the spatial composites, we identify the
282 role of reduced heat transport, decreased evaporation from the ocean surface, and increased downward
283 short-wave radiation behind the MHWs genesis over the western Indian Ocean region. We find the
284 release of upward sensible heat flux and latent heat flux from the ocean after 3–5 days of the MHWs
285 genesis reduce the ocean temperature and play a vital role in the termination of MHWs events. This
286 analysis is also done with ERA5 datasets, and spatial plots of all variables are shown in the
287 supplementary information (Figure S1).

288 To explore the ocean dynamics involved in the genesis of MHWs over the western Indian
289 Ocean region, we performed an oceanic mixed layer heat budget analysis (Figure 6 a, b, c). We
290 calculated the composites of the heat budget terms for the five days before the onset of MHWs (5-day
291 average). The heat budget analysis is carried out for the MHWs between 1994–2015, based on the
292 availability of hydrographic data. Figure 6a, b shows the role of the advection terms and the heat flux
293 terms on the rate of change of SST in the western Indian Ocean region. In the advection term, the heat
294 transport by the zonal ocean currents (the zonal advection term) is dominant compared to the
295 meridional component.

296 In comparison to the advection term, the heat flux term is found to be contributing more to the
297 temperature change. In the net heat flux term, the net solar radiation received in the mixed layer and
298 the latent heat stored (due to less evaporation) in the mixed layer are the major contributors. The solar

299 heating of the ocean surface and decreased evaporative cooling favors the genesis of MHWs in the
300 western Indian Ocean region. The time-integrated heat budget terms in Figure 6c reveal the time
301 evolution of different heat budget parameters.

302 In the north Bay of Bengal region, reduced wind speed anomalies and evaporation lead the
303 MHWs genesis by ~ 2 days ($r=-0.38$) (Figure 5a). Due to weakened wind speed, evaporative cooling
304 over the ocean surface becomes less, and hence the SST increases. An increased OLR and downward
305 solar radiation lead SST by ~ 4 days with r values 0.28 and 0.31, respectively. Hence, the reduced
306 evaporative cooling and increased incoming solar insolation (clear sky conditions) jointly raise the
307 SSTs over the north Bay of Bengal region leading to the MHWs. From the spatial composites in Figure
308 5b, the SST shows a rapid increase coinciding with the MHW genesis day. It is seen that the
309 northeasterly winds establish in the north Bay of Bengal region 5 days before the onset of MHW and
310 weaken the southwesterlies over the particular region. This reduced wind speed leads to a decrease in
311 evaporation at the ocean surface, in turn reducing the release of upward latent heat flux from the ocean.
312 A negative latent heat flux anomaly in the north Bay of Bengal region is observed 5 days before the
313 onset of MHWs, confirming these results. Moreover, there is an increased downward solar radiation
314 and increased OLR one week before the genesis of MHWs, peaking on the starting day of MHWs. We
315 can infer that the decreased upward latent heat flux due to the decreased wind speed and the clear sky
316 condition (increased downward short-wave radiation) contribute to the MHW genesis in the north Bay
317 of Bengal region. After 3 days of the MHW genesis, there is a release of sensible heat and upward
318 longwave radiation from the ocean, reducing the ocean temperature and helping terminate MHWs
319 events. This analysis is also done with ERA5 datasets, and spatial plots of all variables are shown in
320 the supplementary information (Figure S2).

321 It is worth noting that (Figures 6d, e, f) in the northern Bay of Bengal, the temperature change
322 is mainly attributed to the net heat flux, and there is less contribution from the heat advection term.
323 The latent heat (due to decreased evaporation) and net solar radiation have a prominent role among the

heat flux terms. Meanwhile, the role of advection is minimal here. In a nutshell, it can be inferred that the weak wind causes decreased evaporative cooling of the ocean, while the increased solar heating is also accompanying the temperature rise in this region. Figure 6f represents the time-integrated heat budget terms. It is evident that for the north Bay of Bengal region, the MHW duration is comparatively less than the western Indian Ocean region. The heat budget analysis is supplemented with ERA5 radiation datasets (Figure S4). For ERA5 in the western Indian Ocean region, it is noted that the contribution of heat flux terms is less compared with the advection terms. In summary, the role of reduced wind speed and evaporation is more prominent in north Bay of Bengal MHWs, than the western Indian Ocean MHWs.

3.5 Interaction of marine heatwaves with the Indian summer monsoon

The analysis in this section is focused on the summer monsoon rainfall variations during the MHWs over both the western Indian Ocean and north Bay of Bengal regions. We analyzed the mean pattern of SST, vertical velocity (omega at 500 hPa), wind (at 850 hPa), OLR, and vertically integrated moisture flux and the rainfall. It is fascinating that the MHWs over the two regions have the opposite impacts on Indian summer monsoon rainfall.

The SST anomaly composite during western Indian Ocean MHWs shows a warming pattern in this region. The SST anomalies vary from 0.9°C–1.2°C (Figure 7a). Moreover, negative omega (vertical velocity) anomalies at 500 hPa and OLR confirm enhanced convective activity during MHW days over the western Indian Ocean MHW region. Higher SST triggers the ascending motion of air and convection (Figure 7c, Figure S5a). At the same time, the circulation pattern shows strong northeasterly wind anomalies, indicating that the mean southwesterly monsoon winds are weak during this time (Figure S5a). The anomalous Hadley circulation during western Indian Ocean MHW events shows increased convective activities over the equatorial Indian Ocean, while the descending branch occurs over the Indian subcontinent (Figure 7g). This indicates that the western Indian Ocean MHWs

are conducive for inducing dry conditions over the Indian landmass. The vertically integrated moisture flux divergence analysis contributes a more precise picture, suggesting an anomalous moisture flux divergence over the Indian subcontinent, with the moisture transported away towards the western Indian Ocean region (Figure 7e). The mean pattern of rainfall over Indian landmass agrees with the results, with reduced rainfall across most of the subcontinent where the monsoon westerlies are prominent (Figure 7i).

In Figure 7b, the higher SST anomalies in the north Bay of Bengal region are apparent during June–September MHWs. The positive omega anomalies at 500 hPa and the positive OLR values imply dry subsidence and absence of cloud cover (clear sky condition) in this region during strong MHW events (Figure 7d, Figure S5b). However, negative OLR anomalies (above -15 W m^{-2}) and negative omega anomalies at 500 hPa level over the western India and adjacent ocean region suggest enhanced convection and strong ascending motion in these regions. The vertically integrated moisture flux anomalies (Figure 7f) indicate a convergence of the wind in the same region where the OLR and omega anomalies are negative.

Figure 7h shows the mean meridional circulation averaged over the 41°E – 100°E for the north Bay of Bengal region during the June–September MHW days for the period 1982–2018. Over the southern part of the Indian subcontinent (0 – 15°N), there is increased convection during MHW days, supporting the previous results, while there is a suppressed convection at the 20°N due to the dry subsidence over north Bay of Bengal. We find an anomalous moisture flux convergence over the Indian landmass and anomalous moisture flux divergence over the north Bay of Bengal, which provides the cause for the observed rainfall pattern. The moisture transport from the warm north Bay of Bengal region by the anomalous easterly winds plays a crucial role in enhancing the rainfall over the south peninsular Indian subcontinent. There is a convergence of southwesterly monsoon winds and anomalous easterly winds from the Bay of Bengal at 850 hPa over the south-west Indian subcontinent (Figure S5b). The moisture convergence introduces the convective instability over this region. To

summarize, there is a significant relationship between the MHWs in the northern Bay of Bengal and increased summer monsoon rainfall over southwest India.

3.5 Conclusion

Here we have conducted a detailed investigation of the trends and genesis of MHW events in the tropical Indian Ocean—and its interaction with the Indian summer monsoon. We find that the trend in annual frequency of MHWs is relatively higher in the western equatorial Indian Ocean (41°E – 56°E , 8°S – 8°N), which experienced 66 events during the 1982–2018 periods. We further studied the trend in MHW frequency during the Indian summer monsoon period (June–September) and find that the trend in MHWs is prominent in the western Indian Ocean and the north Bay of Bengal (85°E – 93°E , 15°N – 23°N). The north Bay of Bengal experienced 94 MHW events, wherein 34 events occurred from June to September, while in the western Indian Ocean region, it was 21 events.

We further investigated the climate modes driving the MHWs over these two regions. It is observed that the long-term persistence of MHWs in the western Indian Ocean region is associated with the background SST warming primarily identified with the Indian Ocean basin-wide warming (IOB) and also the El Niño, IOD, and NAO. For the north Bay of Bengal MHWs, the longer duration of these events is linked to the IOB, El Niño, and NAO. Earlier studies have pointed that El Niño, IOD and IOB are major contributors to anomalous warm SST events in the tropical ocean (Holbrook et al., 2019). Notably, the SST trend due to global warming is manifested through the increased number of MHW events.

We investigated the seasonal climatology of MHW metrics in both the selected regions. For the western Indian Ocean region, it is found that all the MHWs metrics have a double peak in the seasonal climatology during March and September months. The highest number of western Indian Ocean MHWs events occur in October. For the north Bay of Bengal, all the metrics show high variability during February or May. The highest number of north Bay of Bengal MHWs events occur

399 during May and October months (12 and 14 events, respectively). Interestingly, these two months
400 (May and October) are when the cyclones are active in the Bay of Bengal. Warm SSTs set an ideal
401 precondition for cyclones, and it is hence necessary to closely monitor the basin to understand how
402 these MHWs are interacting with the cyclones.

403 Focusing on the factors influencing the genesis of MHWs events in the tropical Indian Ocean,
404 the results here show that in the western Indian Ocean region, MHWs are formed due to a relaxation
405 of winds prior to the event. This tranquility in the winds is making the SST rise through two ways—
406 through a decrease in the evaporative cooling at the ocean surface, and through a weakened transport
407 of the heat by ocean currents. Apart from this, increased solar heating of the ocean surface due to
408 reduced cloud cover also helps the formation of a warm pool in the western Indian Ocean region. We
409 find that solar insolation plays a major role in MHW genesis from ocean mixed layer heat budget
410 analysis. The reduced upward latent heat flux and zonal heat advection are the other major contributors.
411 Interestingly, we observe an occurrence of cold SST (north of the western Indian Ocean region) region
412 35~40 days prior to western Indian Ocean MHWs and a relatively low SST gradient. This low SST
413 gradient and cold pool may be the reason for the weakening of cross-equatorial flow. The genesis of
414 MHWs in the Tasman Sea and China's marginal seas also had a similar role of ocean dynamics (Oliver
415 et al., 2017, Yao et al., 2020).

416 For the north Bay of Bengal region, it is observed that the reduction in wind speed and thereby
417 reduction in the release of latent heat is one of the major causes for MHW genesis. Along with this,
418 the increased solar radiation at the ocean surface also plays a key role. However, unlike the western
419 Indian Ocean region, the signature of heat advection behind the genesis of MHWs is absent in the case
420 of the north Bay of Bengal. In this study, we find that the western Indian Ocean MHWs have a longer
421 persistence time, and the process of genesis is also slower than the MHWs in the north Bay of Bengal.

422 The MHWs in the western Indian Ocean and the north Bay of Bengal have strong links to the
423 observed variability of the Indian summer monsoon rainfall. We find that both the MHWs are

associated with the drying conditions over the central Indian subcontinent. However, there is a significant increase in the rainfall over south peninsular India in response to the MHWs in the north Bay of Bengal. Climate model projections suggest further warming of the Indian Ocean in the future, which will very likely intensify the MHWs (Collins et al., 2019) and their impact on the monsoon rainfall. Since the frequency, intensity, and area of marine heatwaves are increasing, it is essential that we closely monitor and forecast these events in advance in order to mitigate their impacts.

Acknowledgments

The Optimum Interpolated Sea Surface Temperature (OISST) and the Outgoing Longwave Radiation (OLR) are available from National Oceanic and Atmospheric Administration (NOAA) (Reynolds et al., 2007). The daily wind, latent heat flux, sensible heat flux, upward longwave radiation, downward solar radiation, surface net longwave radiation, and surface net solar radiation are available from the National Center for Environmental Prediction/National Centers for Atmospheric Research (NCEP/NCAR) reanalysis data (Kalnay et al., 1996). For the analysis of the rainfall variability over the India, we used daily rainfall available from the Indian Meteorological Department (Pai et al., 2014). The ocean current data is available from the Ocean Surface Current Analysis Real-time (OSCAR), provided by the Earth Space Research (Dohan and Maximenko, 2010).

Author contributions

M.K.R. conceived the study and J.S.S. performed the analysis. J.S.S., M.K.R., and P.D. contributed to the interpretation of the results and drafting of the manuscript for publication. A.A. performed some of the preliminary analysis.

References

Balmaseda, M.A., Trenberth, K.E., Källén, E (2013), Distinctive climate signals in reanalysis of global ocean heat content, *Geophys. Res. Lett.*, 40, 1754–1759, doi:1002/grl.50382.

- 450 Beal, L.M., Vialard, J., Roxy, M.K., Li, J., Andres, M., Annamalai, H., Feng, M., Han, W., Hood, R.,
451 Lee, T. and Lengaigne, M., 2020. A Road Map to IndOOS-2: Better Observations of the
452 Rapidly Warming Indian Ocean. *Bull. Am. Meteorol. Soc.*, 101(11), pp.E1891-E1913.
- 453 Benthuisen, J.A., Tonin, H., Brinkman, R., Herzfeld, M., Steinberg, C (2016), Intrusive upwelling in
454 the Central Great Barrier Reef, *J. Geophys. Res. Oceans*, 121, 8395–8416,
455 doi:10.1002/2016JC012294.
- 456 Chen, K., Gawarkiewicz, G., Kwon, Y.O., and Zhang, W.G. (2015), The role of atmospheric forcing
457 versus ocean advection during the extreme warming of the Northeast US continental shelf in
458 2012, *J. Geophys. Res. Oceans*, 120(6), 4324–4339.
- 459 Collins M., M. Sutherland, L. Bouwer, S.-M. Cheong, T. Frölicher, H. Jacot Des Combes, M. Koll
460 Roxy, I. Losada, K. McInnes, B. Ratter, E. Rivera-Arriaga, R.D. Susanto, D. Swingedouw, and
461 L. Tibig, 2019: Extremes, Abrupt Changes and Managing Risk. In: IPCC Special Report on
462 the Ocean and Cryosphere in a Changing Climate [H.-O. Pörtner, D.C. Roberts, V. Masson-
463 Delmotte, P. Zhai, M. Tignor, E. Poloczanska, K. Mintenbeck, A. Alegría, M. Nicolai, A.
464 Okem, J. Petzold, B. Rama, N.M. Weyer (eds.)].
- 465 Darmaraki, S., Somot, S., Sevault, F., Nabat, P., Cabos Narvaez, W.D., Cavicchia, L., Djurdjevic, V.,
466 Li, L., Sannino, G., Sein, D.V (2019), Future evolution of Marine Heatwaves in the
467 Mediterranean Sea, *Clim. Dyn.*, 53, 1371–1392, doi:10.1007/s00382-019-04661-z.
- 468 Dohan, K., Maximenko, N (2010), Monitoring Ocean Currents with Satellite Sensors, *Oceanography*,
469 23, 94–103, doi:10.5670/oceanog.2010.08.
- 470 Edward, J.P., Mathews, G., Raj, K.D., Laju, R.L., Bharath, M.S., Arasamuthu, A., Kumar, P.D., Bilgi,
471 D.S. and Malleshappa, H., 2018. Coral mortality in the Gulf of Mannar, southeastern India, due
472 to bleaching caused by elevated sea temperature in. *Curr. Sci.*, 114(9), p.1967.
- 473 Elzahaby, Y., Schaeffer, A (2019), Observational Insight Into the Subsurface Anomalies of Marine
474 Heatwaves, *Front. Mar. Sci.*, 6, doi:10.3389/fmars.2019.00745.
- 475 Foltz, G.R., Grodsky, S.A., Carton, J.A. and McPhaden, M.J., 2003. Seasonal mixed layer heat budget
476 of the tropical Atlantic Ocean. *J. Geophys. Res. Oceans*, 108(C5).
- 477 Frölicher, T.L (2019), Chapter 5 - Extreme climatic events in the ocean, in: Cisneros-Montemayor,
478 A.M., Cheung, W.W.L., Ota, Y. (Eds.), Predicting Future Oceans, *Elsevier*, 53–60,
479 doi:10.1016/B978-0-12-817945-1.00005-8.
- 480 Frölicher, T.L., Fischer, E.M., Gruber, N, (2018), Marine heatwaves under global warming, *Nature*,
481 560, 360–364, doi:10.1038/s41586-018-0383-9.
- 482 Hersbach, H. and Dee, D.J.E.N., 2016. ERA5 reanalysis is in production. *ECMWF newsletter*, 147(7),
483 pp.5-6.
- 484 Hobday, A.J., Alexander, L.V., Perkins, S.E., Smale, D.A., Straub, S.C., Oliver, E.C.J., Benthuisen,
485 J.A., Burrows, M.T., Donat, M.G., Feng, M., Holbrook, N.J., Moore, P.J., Scannell, H.A., Sen
486 Gupta, A., Wernberg, T (2016), A hierarchical approach to defining marine heatwaves, *Prog.*
487 *Oceanogr.*, 141, 227–238, doi:10.1016/j.pocean.2015.12.014.
- 488 Holbrook, N.J., Scannell, H.A., Gupta, A.S., Benthuisen, J.A., Feng, M., Oliver, E.C.J., Alexander,
489 L.V., Burrows, M.T., Donat, M.G., Hobday, A.J., Moore, P.J., Perkins-Kirkpatrick, S.E.,

490 Smale, D.A., Straub, S.C., Wernberg, T (2019), A global assessment of marine heatwaves and
491 their drivers, *Nat. Commun.*, 10, 1–13, doi:10.1038/s41467-019-10206-z.

492 IPCC, 2019: IPCC Special Report on the Ocean and Cryosphere in a Changing Climate [H.-O. Pörtner,
493 D.C. Roberts, V. Masson-Delmotte, P. Zhai, M. Tignor, E. Poloczanska, K. Mintenbeck, A.
494 Alegría, M. Nicolai, A. Okem, J. Petzold, B. Rama, N.M. Weyer (eds.)].

495 Jackson, J.M., Johnson, G.C., Dosser, H.V., Ross, T (2018), Warming From Recent Marine Heatwave
496 Lingers in Deep British Columbia Fjord, *Geophys. Res. Lett.*, 45, 9757–9764,
497 doi:10.1029/2018GL078971.

498 Joh, Y., Lorenzo, E.D (2017), Increasing Coupling Between NPGO and PDO Leads to Prolonged
499 Marine Heatwaves in the Northeast Pacific, *Geophys. Res. Lett.*, 44, 11,663-11,671,
500 doi:10.1002/2017GL075930.

501 Kalnay, E., Kanamitsu, M., Kistler, R., Collins, W., Deaven, D., Gandin, L., Iredell, M., Saha, S.,
502 White, G., Woollen, J. and Zhu, Y., 1996. The NCEP/NCAR 40-year reanalysis project. *Bull.*
503 *Amer. Meteor.*, 77(3), pp.437-472.

504 Krishnan, P., Roy, S.D., George, G., Srivastava, R.C., Anand, A., Murugesan, S., Kaliyamoorthy, M.,
505 Vikas, N., Soundararajan, R (2011), Elevated sea surface temperature during May 2010 induces
506 mass bleaching of corals in the Andaman, *Curr. Sci.*, 100, 111–117.

507 Laufkötter, C., Zscheischler, J. and Frölicher, T.L., 2020. High-impact marine heatwaves attributable
508 to human-induced global warming. *Science*, 369(6511), pp.1621-1625.

509 Liebmann, B., & Smith, C. A. (1996). Description of a complete (interpolated) outgoing longwave
510 radiation dataset. *Bull. Am. Meteorol. Soc.*, 77(6), 1275-1277.

511 Metzger, E.J., Smedstad, O.M., Thoppil, P.G., Hurlburt, H.E., Cummings, J.A., Wallcraft, A.J.,
512 Zamudio, L., Franklin, D.S., Posey, P.G., Phelps, M.W. and Hogan, P.J., 2014. US Navy
513 operational global ocean and Arctic ice prediction systems. *Oceanography*, 27(3), pp.32-43.

514 Mills, K.E., Pershing, A.J., Brown, C.J., Chen, Y., Chiang, F.-S., Holland, D.S., Lehutha, S., Nye, J.A.,
515 Sun, J.C., Thomas, A.C., Wahle, R.A (2013), Fisheries Management in a Changing Climate:
516 Lessons from the 2012 Ocean Heat Wave in the Northwest Atlantic, *Oceanography*, 26, 191–
517 195.

518 Oliver, E.C., Benthuisen, J.A., Bindoff, N.L., Hobday, A.J., Holbrook, N.J., Mundy, C.N., and
519 Perkins-Kirkpatrick, S.E (2017), The unprecedented 2015/16 Tasman Sea marine heatwave,
520 *Nat.Comm.*, 8(1), 1-12.

521 Oliver, E.C., Burrows, M.T., Donat, M.G., Sen Gupta, A., Alexander, L.V., Perkins-Kirkpatrick, S.E.,
522 Benthuisen, J., Hobday, A.J., Holbrook, N.J., Moore, P.J. and Thomsen, M.S., 2019. Projected
523 marine heatwaves in the 21st century and the potential for ecological impact. *Front. Mar. Sci.*
524 6, p.734.

525 Oliver, E.C.J., Donat, M.G., Burrows, M.T., Moore, P.J., Smale, D.A., Alexander, L.V., Benthuisen,
526 J.A., Feng, M., Gupta, A.S., Hobday, A.J., Holbrook, N.J., Perkins-Kirkpatrick, S.E., Scannell,
527 H.A., Straub, S.C., Wernberg, T. 2018a , Longer and more frequent marine heatwaves over the
528 past century, *Nat. Commun.*, 9, 1–12, doi: 10.1038/s41467-018-03732-9.

529 Pai, D.S., Sridhar, L., Rajeevan, M., Sreejith, O.P., Satbhai, N.S. and Mukhopadhyay, B., 2014.
530 Development of a new high spatial resolution (0.25× 0.25) long period (1901–2010) daily
531 gridded rainfall data set over India and its comparison with existing data sets over the region.
532 *Mausam*, 65(1), pp.1-18.

533 Piatt, J.F., Parrish, J.K., Renner, H.M., Schoen, S.K., Jones, T.T., Arimitsu, M.L., Kuletz, K.J.,
534 Bodenstein, B., García-Reyes, M., Duerr, R.S., Corcoran, R.M., Kaler, R.S.A., McChesney,
535 G.J., Golightly, R.T., Coletti, H.A., Suryan, R.M., Burgess, H.K., Lindsey, J., Lindquist, K.,
536 Warzybok, P.M., Jahncke, J., Roletto, J., Sydeman, W.J (2020), Extreme mortality and
537 reproductive failure of common murres resulting from the northeast Pacific marine heatwave
538 of 2014-2016, *PLOS ONE* 15, e0226087, doi:10.1371/journal.pone.0226087.

539 Raj, K.D., Mathews, G., Bharath, M.S., Laju, R.L., Kumar, P.D., Arasamuthu, A. and Edward, J.P.,
540 2018. Cushion star (*Culcitasmidelliana*) preys on coral polyps in Gulf of Mannar, Southeast
541 India. *Mar Freshw Behav Physiol*, 51(2), pp.125-129.

542 Rodrigues, R.R., Taschetto, A.S., Gupta, A.S., Foltz, G.R (2019), Common cause for severe droughts
543 in South America and marine heatwaves in the South Atlantic, *Nat. Geosci.*, 12, 620–626,
544 doi:10.1038/s41561-019-0393-8.

545 Roxy, M.K., Modi, A., Murtugudde, R., Valsala, V., Panickal, S., Prasanna Kumar, S., Ravichandran,
546 M., Vichi, M. and Lévy, M., 2016. A reduction in marine primary productivity driven by rapid
547 warming over the tropical Indian Ocean. *Geophys. Res. Lett.*, 43(2), pp.826-833.

548 Roxy, M.K., Ritika, K., Terray, P., Masson, S (2014), The Curious Case of Indian Ocean Warming, *J.*
549 *Clim.*, 27, 8501–8509, doi:10.1175/JCLI-D-14-00471.1.

550 Roxy, M.K., Ritika, K., Terray, P., Murtugudde, R., Ashok, K., Goswami, B.N (2015), Drying of
551 Indian subcontinent by rapid Indian Ocean warming and a weakening land-sea thermal
552 gradient, *Nat. Commun.*, 6, 1–10, doi:10.1038/ncomms8423.

553 Roxy, M. and Tanimoto, Y., 2012. Influence of sea surface temperature on the intraseasonal variability
554 of the South China Sea summer monsoon. *Clim. Dyn.*, 39(5), pp.1209-1218.

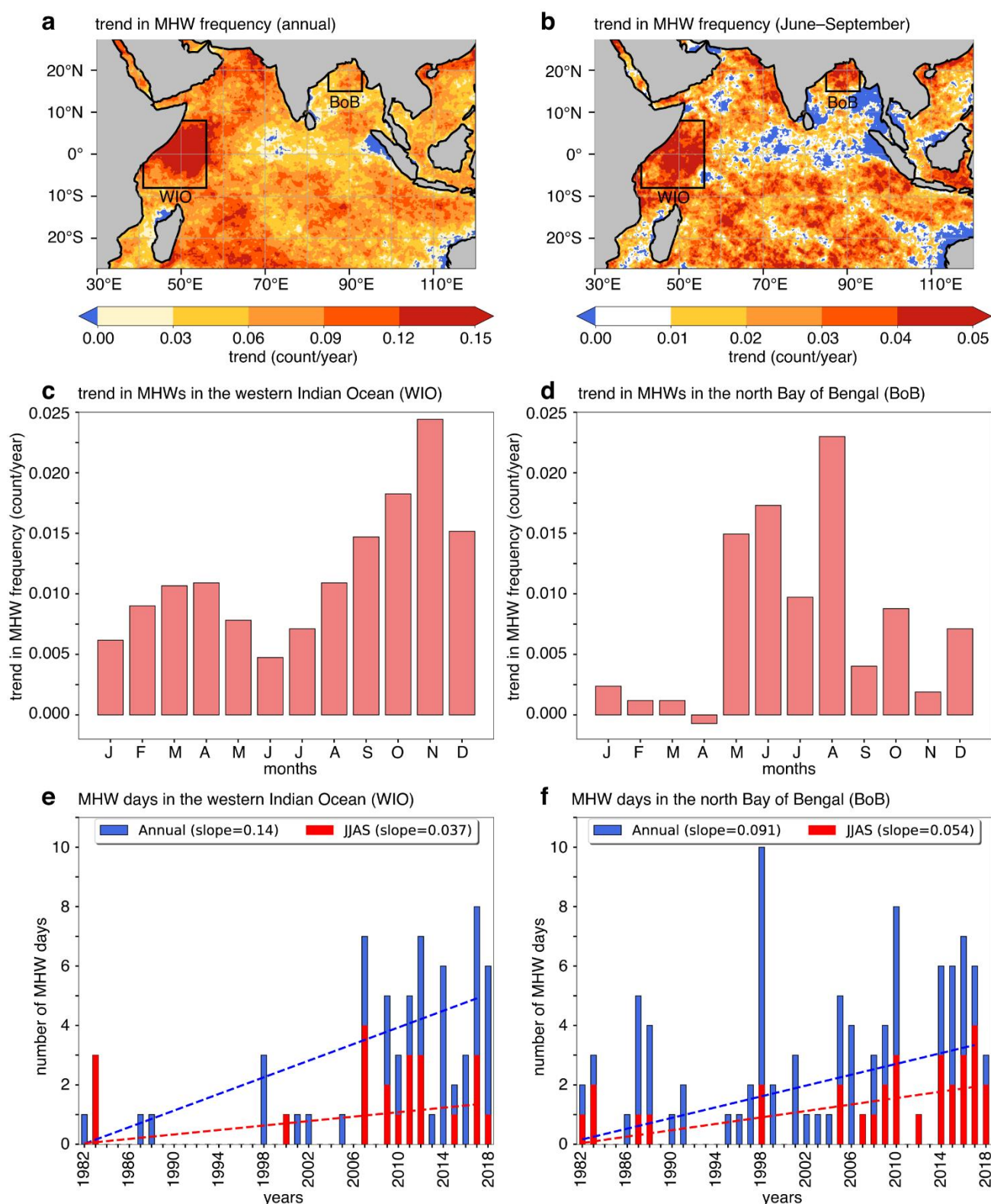
555 Schaeffer, A., Gramouille, A., Roughan, M., Mantovanelli, A (2017), Characterizing frontal eddies
556 along the East Australian Current from HF radar observations, *J. Geophys. Res. Oceans*, 122,
557 3964–3980, doi:10.1002/2016JC012171.

558 Schlegel, R.W., Oliver, E.C.J., Wernberg, T., Smit, A.J (2017), Nearshore and offshore co-occurrence
559 of marine heatwaves and cold-spells, *Prog. Oceanogr.*, 151, 189–205,
560 doi:10.1016/j.pocean.2017.01.004.

561 Singh, C. and Dasgupta, P., 2017. Unraveling the spatio-temporal structure of the atmospheric and
562 oceanic intra-seasonal oscillations during the contrasting monsoon seasons. *Atmos. Res.*, 192,
563 pp.48-57.

564 Walker, H.J., Hastings, P.A., Hyde, J.R., Lea, R.N., Snodgrass, O.E., Bellquist, L.F (2020), Unusual
565 occurrences of fishes in the Southern California Current System during the warm water period
566 of 2014–2018, *Estuar. Coast. Shelf Sci.*, 236, 106634, doi:10.1016/j.ecss.2020.106634.

- 567 Wang, B., Biasutti, M., Byrne, M.P., Castro, C., Chang, C.P., Cook, K., Fu, R., Grimm, A.M., Ha,
568 K.J., Hendon, H. and Kitoh, A., 2020. Monsoons Climate Change Assessment. *Bull. Am.*
569 *Meteorol. Soc.*
- 570 Xie, S.P., Kosaka, Y., Du, Y., Hu, K., Chowdary, J.S. and Huang, G., 2016. Indo-western Pacific ocean
571 capacitor and coherent climate anomalies in post-ENSO summer: A review. *Adv. Atmos. Sci.*,
572 33(4), pp.411-432.
- 573 Yao, Y., Wang, J., Yin, J., Zou, X (2020), Marine Heatwaves in China's Marginal Seas and Adjacent
574 Offshore Waters: Past, Present, and Future, *J. Geophys. Res. Oceans*, 125, e2019JC015801,
575 doi:10.1029/2019JC015801.
- 576 Zhang, N., Feng, M., Hendon, H.H., Hobday, A.J., Zinke, J (2017), Opposite polarities of ENSO drive
577 distinct patterns of coral bleaching potentials in the southeast Indian Ocean, *Sci. Rep.*, 7,
578 doi:10.1038/s41598-017-02688-y.

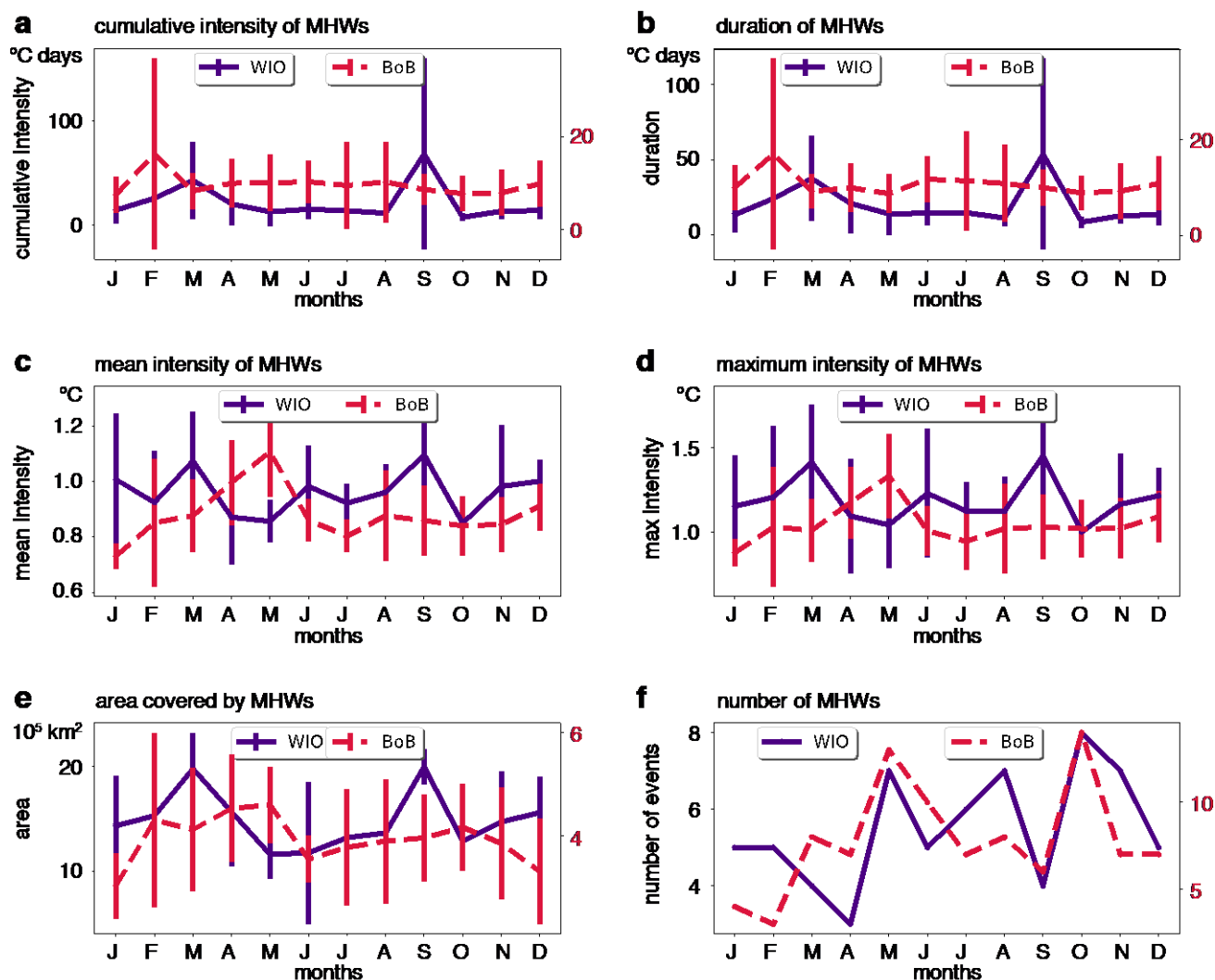


579

580 **Figure 1:** Trend in MHW frequency (count/year) in the Indian Ocean during 1982–2018 (a)
 581 annually and for (b) June–September, using NOAA OISST data. Month-wise trend of MHW
 582 frequency in the (c) western Indian Ocean (WIO, 41°E–56°E, 8°S–8°N) and (d) north Bay of
 583 Bengal (85°E–93°E, 15°N–23°N). Time series of the number of MHW days annually (blue bars),

584 and during June–September (red bars), from 1982–2018 in (e) the western Indian Ocean and (f)
 585 the north Bay of Bengal region. Trend lines in the figure are statistically significant ($p<0.05$).

586



587

588 **Figure 2:** Climatology of MHWs. Month-wise distribution of (a) cumulative intensity (°C days), (b)
 589 mean intensity (°C), (c) duration (days), (d) maximum intensity (°C), (e) area (km²) and (f) the number
 590 of MHW events, during 1982–2018 for the western Indian Ocean (WIO, 41°E–56°E, 8°S–8°N) and
 591 the north Bay of Bengal (BoB, 85°E–93°E, 15°S–23°N). The error bar represents the standard
 592 deviation.

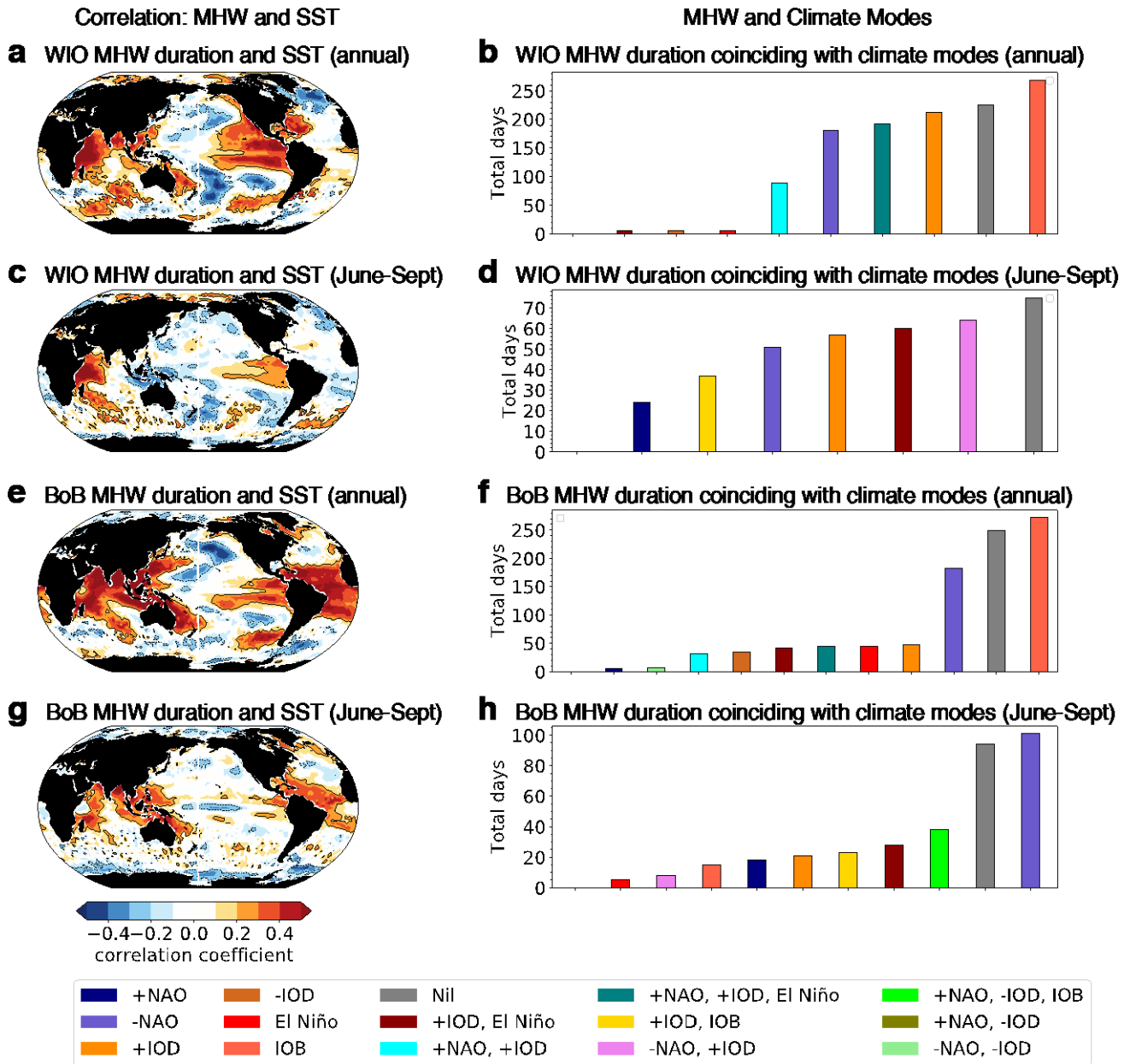
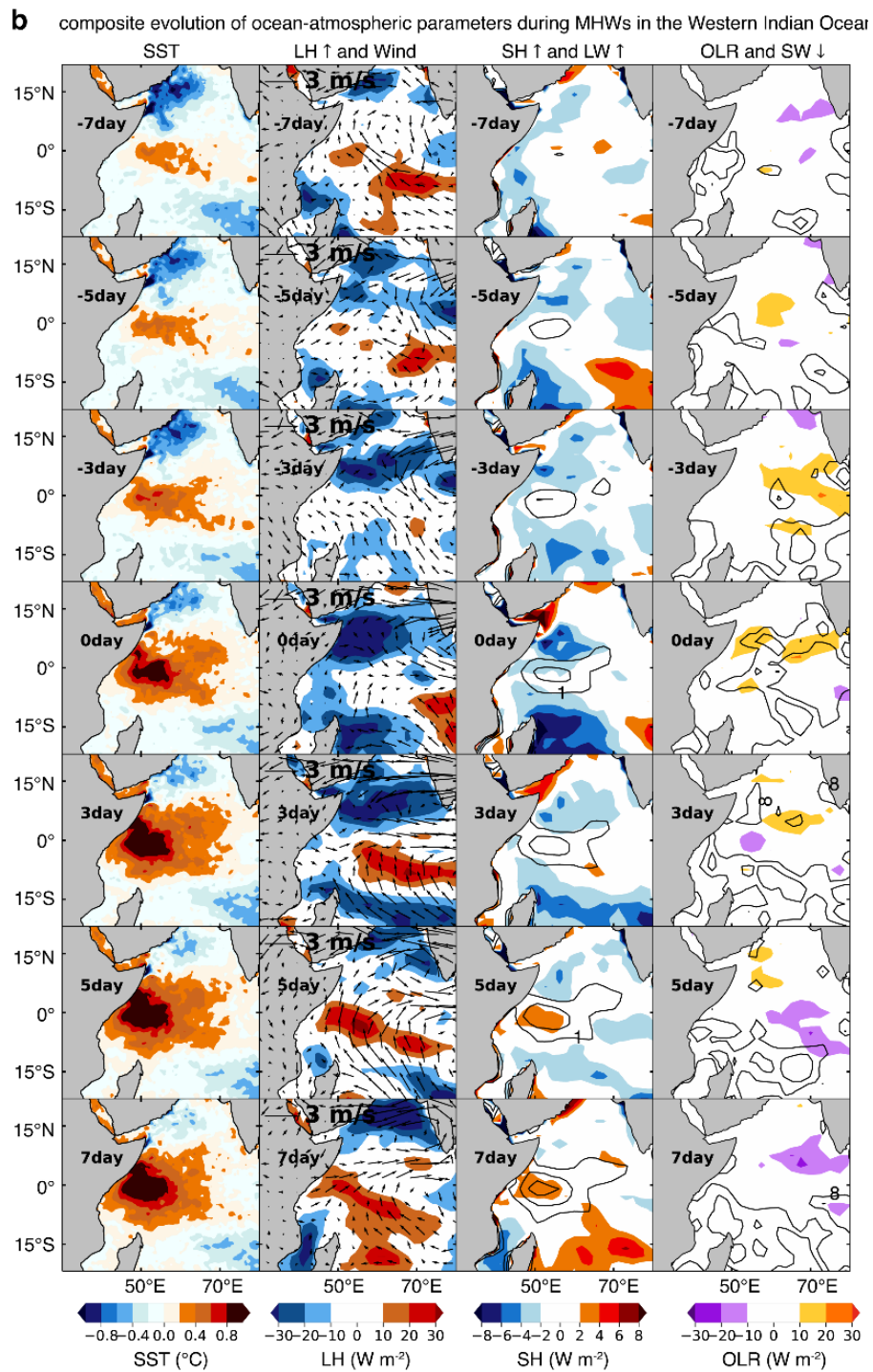
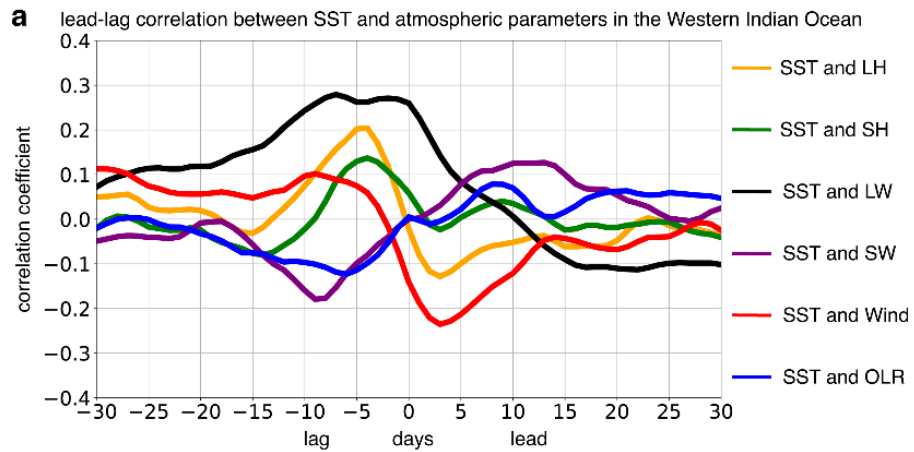
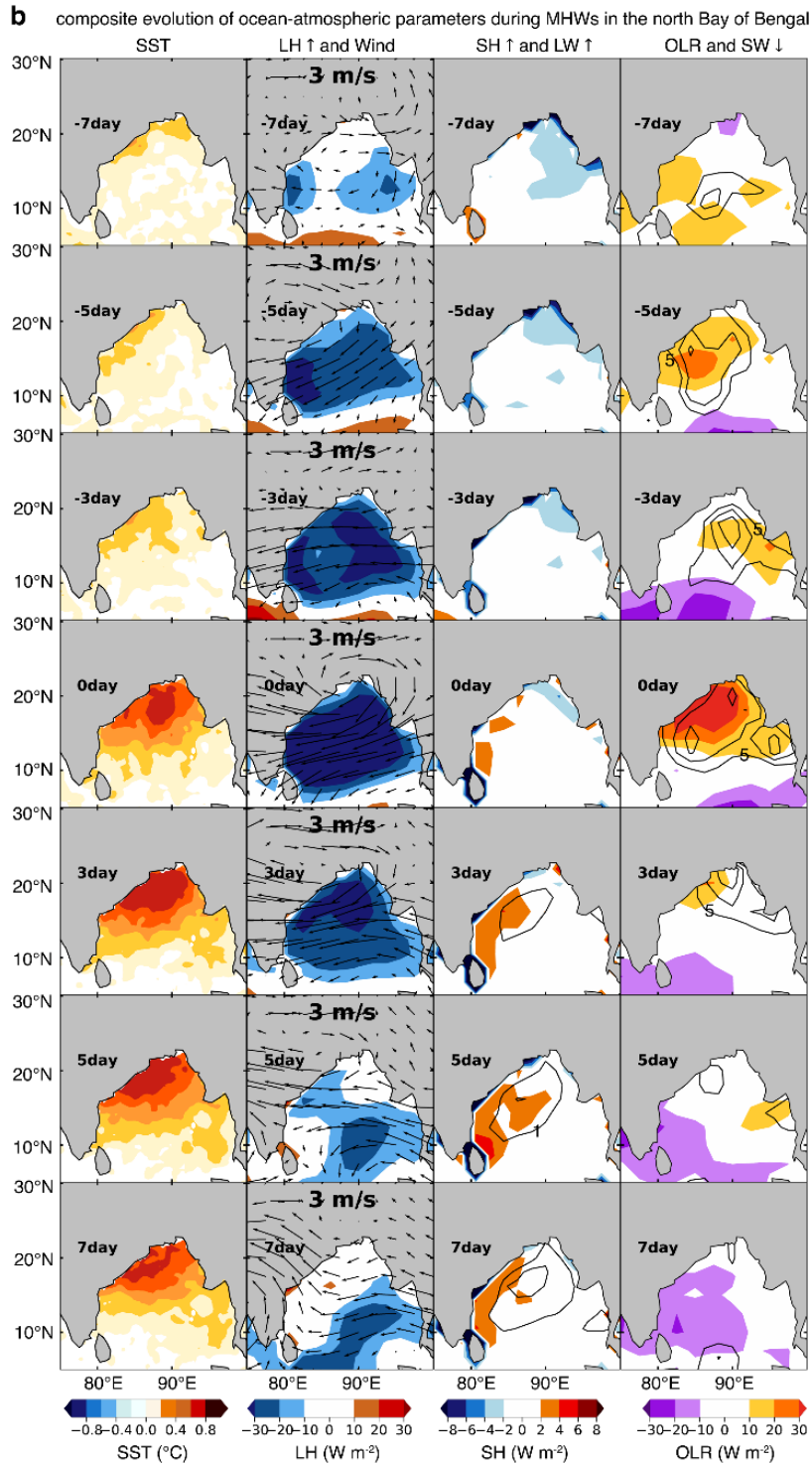
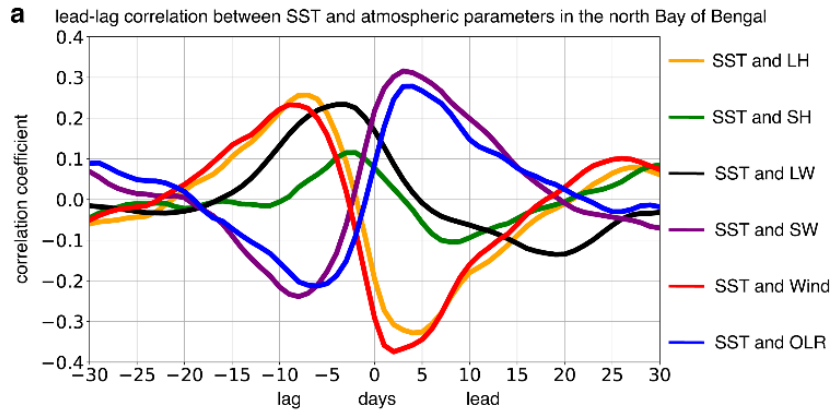


Figure 3: Correlation map between duration of MHWs and global SST for (a, e) annual and (c, g) June to September in the western Indian Ocean (WIO) and the north Bay of Bengal (BoB). The bar-charts (b, d, f, h) indicate the total duration of MHWs coinciding with climate modes. “Nil” means the MHW days that do not coincide with any of the climate modes.



599 **Figure 4:** (a) The lead-lag correlation between SST and wind speed (red line), latent heat flux (orange
600 line), sensible heat flux (green line), upward long wave radiation (black line), OLR (blue line) in the
601 western Indian Ocean, estimated from the 30 days before and 30 days after the genesis of MHW events.
602 Composite evolution of (b) SST ($^{\circ}\text{C}$), latent heat (LH, W m^{-2}), wind (m s^{-1}), OLR (W m^{-2}), shortwave
603 radiation (SW, W m^{-2}), sensible heat (SH, W m^{-2}), and longwave (LW, W m^{-2}), in the western Indian
604 Ocean before and during MHWs for the period 1982–2018, using NCEP/NCAR reanalysis datasets.
605 Upward arrow represents the exchange of flux from ocean to atmosphere and downward arrow
606 represents the exchange of flux from ocean to atmosphere.



608 **Figure 5:** (a) The lead-lag correlation between SST and wind speed (red line), latent heat flux
609 (orange line), sensible heat flux (green line), upward long wave radiation (black line), OLR (blue
610 line) in the north Bay of Bengal, estimated from the 30 days before and 30 days after the genesis
611 of MHW events. Composite evolution of (b) SST ($^{\circ}\text{C}$), latent heat (LH, W m^{-2}), wind (m s^{-1}), OLR
612 (W m^{-2}), shortwave radiation (SW, W m^{-2}), sensible heat (SH, W m^{-2}), and longwave (LW, W m^{-2}),
613 in the western Indian Ocean before and during MHWs for the period 1982–2018, using
614 NCEP/NCAR reanalysis datasets. Upward arrow represents the exchange of flux from ocean to
615 atmosphere and downward arrow represents the exchange of flux from ocean to atmosphere.

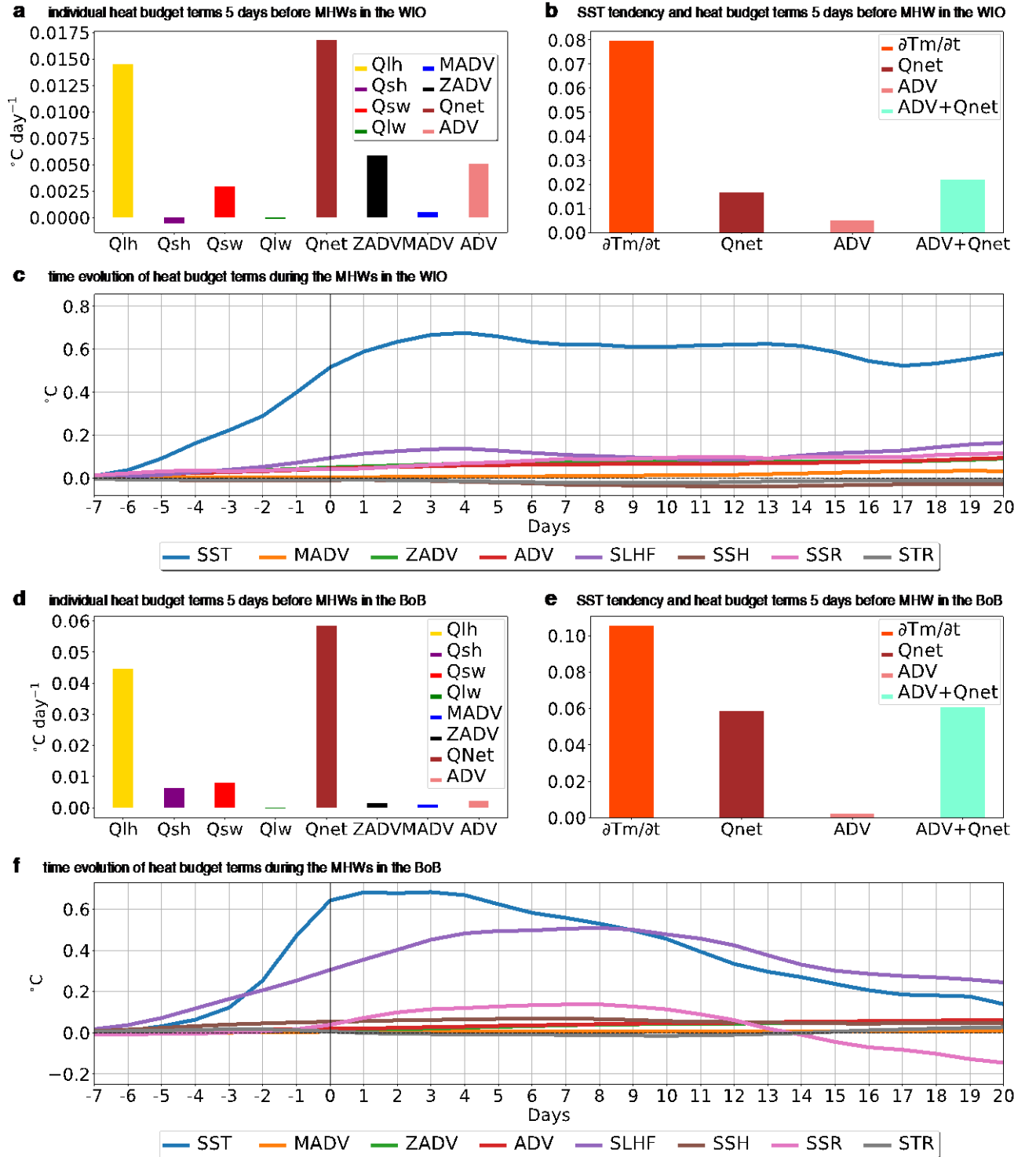


Figure 6: (a, d) Individual heat-budget terms (in $^{\circ}\text{C day}^{-1}$) and (b, e) SST tendency with the heat budget terms 5 days before the genesis of MHW in the western Indian Ocean (WIO) and the north Bay of Bengal (BoB). (c, f) Time evolution of the heat budget terms (in $^{\circ}\text{C}$) during the evolution of MHWs in the WIO and BoB. Heat budget terms estimated using the OSCAR current data and NCEP/NCAR fluxes during 1994–2015.

composite anomaly of ocean-atmospheric conditions during MHW events
western Indian Ocean north Bay of Bengal

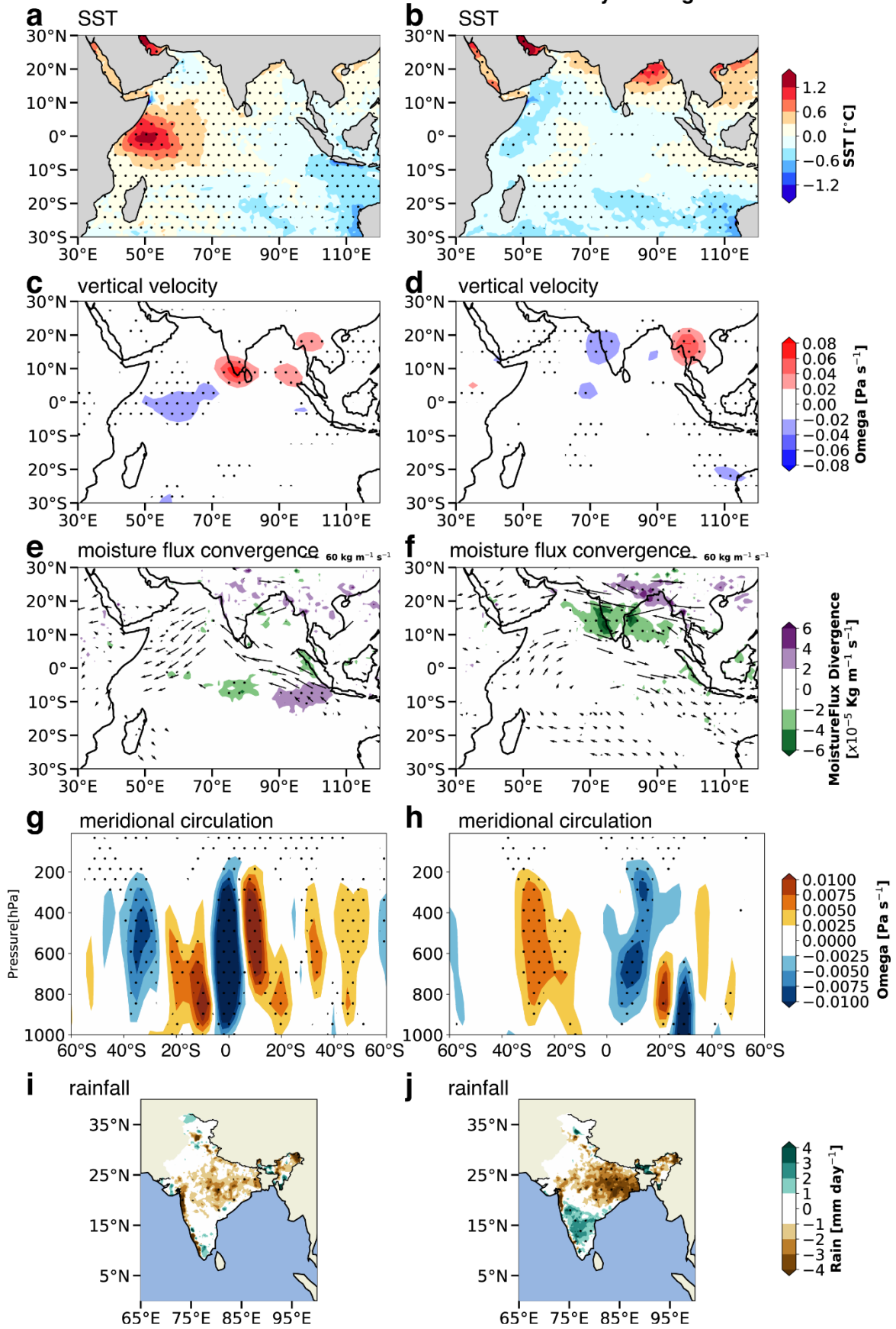


Figure 7: Composite anomaly of daily (a, b) sea Surface Temperature Anomalies (SST, $^{\circ}\text{C}$), (c, d) vertical velocity anomalies (omega at 500 hPa, Pa s^{-1}), (e, f) moisture flux convergence ($\text{kg m}^{-1} \text{s}^{-1}$), (g, h) meridional circulation over 40°E – 100°E (vertical velocity, Pa s^{-1}) and (i, j) rainfall (mm day^{-1}) during MHW days in the western Indian Ocean and north Bay of Bengal, during June–September, for 1982–2018. Stippling (black dots) indicates anomaly values significant at 95% confidence level.

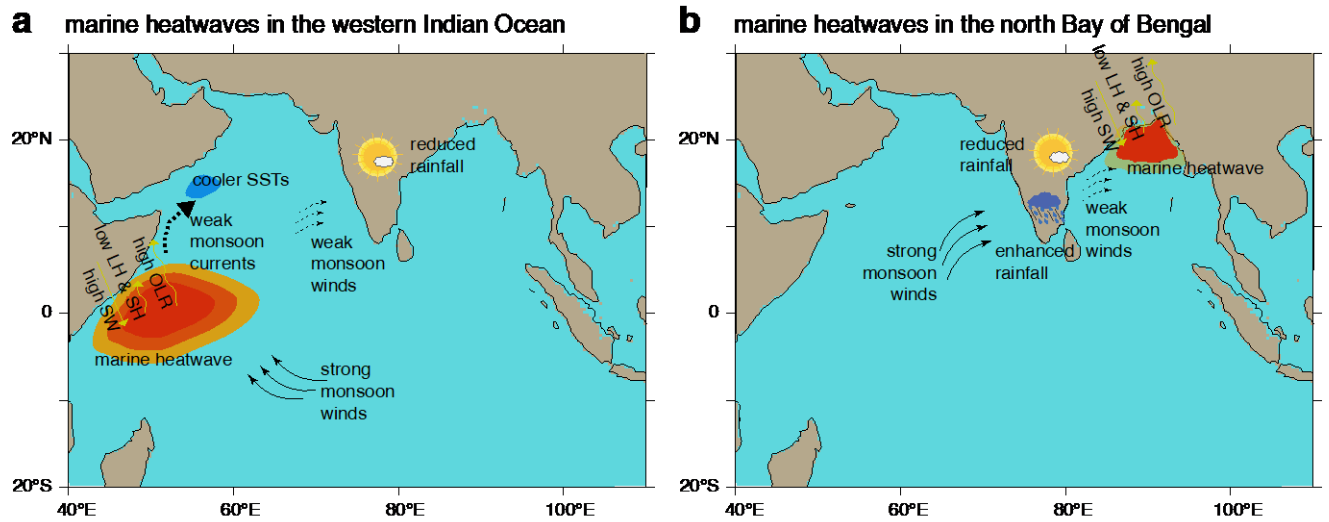


Figure 8: Schematic diagram depicting the factors leading to the genesis of MHW in (a) the western Indian Ocean and (b) the north Bay of Bengal, and its impact on the Indian summer monsoon rainfall.